Evolution of magnetic and structural transitions and enhancement of magnetocaloric effect in $Fe_{1-x}Mn_xV_2O_4$

D. Choudhury,[1] T. Suzuki,[1] D. Okuyama,[1] D. Morikawa,[1] K. Kato,[2] M. Takata,[2] K. Kobayashi,[3] R. Kumai,[3] H. Nakao,[3]
Y. Murakami,[3] M. Bremholm,[4] B. B. Iversen,[4] T. Arima,[1,2,5] Y. Tokura,[1,6] and Y. Taguchi[1]

[1]*RIKEN Center for Emergent Matter Science (CEMS), Wako 351-0198, Japan*
[2]*RIKEN SPring-8 Center, 1-1-1 Kouto, Sayo-cho, Sayo-gun, Hyogo 679-5148, Japan*
[3]*Condensed Matter Research Center and Photon Factory, Institute of Materials Structure Science,
High Energy Accelerator Research Organization, Tsukuba, Ibaraki 305-0801, Japan*
[4]*Center for Materials Crystallography, Department of Chemistry and iNANO, Aarhus University, DK-8000, Aarhus C, Denmark*
[5]*Department of Advanced Materials Science, University of Tokyo, Kashiwa 277-8561, Japan*
[6]*Department of Applied Physics, University of Tokyo, Tokyo 113-8656, Japan*

Magnetic, structural, and magnetocaloric properties have been investigated for a solid-solution system, $Fe_{1-x}Mn_xV_2O_4$ ($0.0 \leqslant x \leqslant 1.0$) with a spinel structure. As orbital-active Fe^{2+} ions are partially substituted with orbital-inactive Mn^{2+} ions, various interactions, such as the Jahn–Teller interaction, spin-orbit coupling, and the exchange interaction, compete with each other, giving rise to a rich magnetic and structural phase diagram. The magnetocaloric effect exhibits two peaks as a function of temperature for $x \leqslant 0.9$, associated with a higher-temperature ferrimagnetic transition, and with a lower-temperature concomitant spin-canting and orbital-ordering (mostly lattice-structural) transition of the V site. The large magnetocaloric effect as observed in MnV_2O_4 can thus be attributed to the sum of the entropy changes upon the merged phase transition at $T_{N1} \sim T_{N2}$.

PACS number(s): 71.27.+a, 75.50.−y, 75.30.Sg

Transition-metal oxides with spinel structure have attracted much research attention over many years because these compounds exhibit intriguing physical phenomena, such as orbital ordering, geometrically frustrated magnetism, and charge ordering [1–6], due to an intricate coupling among their orbital, spin, and charge degrees of freedom. These compounds consist of two distinct cation sites: a tetrahedrally coordinated *A* site and an octahedrally coordinated *B* site, as schematically shown in Fig. 1(a). The *B* sites form a network of corner-sharing tetrahedra, giving rise to the geometric frustration. The rich physics of the spinel compounds arises from various possible combinations of spin, charge, and orbital degrees of freedom of the *A*-site and *B*-site cations and their coupling to the lattice [7,8].

Amongst spinels, FeV_2O_4 is a rare example endowed with orbital degrees of freedom at both the *A* site (Fe^{2+} with $S = 2$) and *B* site (V^{3+} with $S = 1$). At room temperature, the system has a cubic structure, and one down-spin electron of Fe^{2+} is accommodated in doubly degenerate e_g levels, and two electrons of V^{3+} occupy two of the triply degenerate t_{2g} orbitals [9]. This material undergoes multiple magnetic and structural transitions [10–12]. As shown in the phase diagram [Fig. 2(a)] based on our present results, FeV_2O_4 exhibits a cooperative Jahn–Teller distortion driven by Fe^{2+} at $T_s = 138$ K from cubic to compressed tetragonal (T1) phase with $c < a$ lattice parameters, where the degeneracy of e_g levels is lifted [10,11]. At $T_{N1} = 117$ K, a magnetic transition occurs where Fe and V spins align in a collinear ferrimagnetic configuration, accompanied by a structural transition into an orthorhombic (O) phase due to the spin-orbit interaction of Fe^{2+}. Further lowering of the temperature to $T_{N2} = 64$ K induces a V-spin canting transition to form a "two-in, two-out" structure [12], and the crystal structure changes simultaneously into an elongated tetragonal (T2) phase with $c > a$. It was recently

demonstrated that a ferroic ordering of complex orbital ($|yz\rangle + i|zx\rangle$ type) at the V sites also occurs below the spin-canting transition [11,13]; the proposed orbital configuration [11] at the ground state is displayed in Fig. 1(b).

Another end compound, MnV_2O_4, is also an interesting material which has been extensively investigated [11,14–19]. In this material, the V^{3+} state has an orbital degree of freedom while Mn^{2+} with $S = 5/2$ does not. A spin-collinear ferrimagnetic transition occurs at $T_{N1} = 57$ K, and then around $T_{N2} = 54$ K a simultaneous spin-canting and antiferro-orbital-ordering transition of the V site takes place, accompanied by a compressed tetragonal distortion due to exchange striction and Jahn–Teller coupling at the V site [11,15]. At around $T_{N1} \sim T_{N2}$, a large magnetocaloric effect has been observed [20]. Figure 1(b) shows a schematic orbital configuration at the ground state of MnV_2O_4 as well, which is reported in Ref. [11]. It will thus be of significant interest to investigate the solid-solution system that connects both end members and to clarify the evolution of magnetic and structural transitions, in the light of the interplay of various interactions at both the *A* site and *B* site.

For this paper, we systematically studied the magnetic and structural properties as well as the magnetocaloric effect of the solid-solution system $Fe_{1-x}Mn_xV_2O_4$. The magnetocaloric effect, evaluated as an isothermal entropy change [$-\Delta S \equiv S(T, H = 0) - S(T, H)$] upon application of a magnetic field H, has actively been investigated recently as a possible alternative refrigeration technique [21–23]. We have found moderately large values of $-\Delta S$ associated with the two magnetic transitions, and also nonmonotonic x dependence of ΔS upon the simultaneous spin-canting and orbital-ordering transition of V electrons. The present systematic investigation revealed that the large value previously observed for the end compound MnV_2O_4 [20] can be ascribed to the sum of the
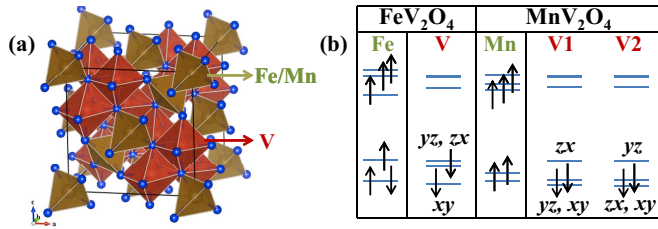
FIG. 1. (Color online) (a) Schematic of spinel structure composed of tetrahedral AO_4 (A = Fe, Mn) and octahedral VO_6 units. (b) Ground-state (i.e., $T < T_{N2}$) spin and orbital configuration of Fe^{2+}, Mn^{2+}, and V^{3+} ions in FeV_2O_4 and MnV_2O_4 as reported in Ref. [11]. Two electrons of V site uniformly occupy $|xy\rangle$ state and $|yz\rangle + i|zx\rangle$ state in the case of FeV_2O_4 while alternately occupying $|xy\rangle$ and $|yz\rangle$ states at V1 site, and $|xy\rangle$ and $|zx\rangle$ states at the V2 site in the case of MnV_2O_4, where V1 and V2 sites are the two sites connected with 4_1 operation in the T3 phase with $I4_1/a$ space group. Note that the notation for the crystal axes here is different from that used in Ref. [11], but the same as in Ref. [18].

two transitions at $T_{N1} \sim T_{N2}$, providing an important strategy to obtain a large magnetocaloric effect.

$Fe_{1-x}Mn_xV_2O_4$ samples were synthesized by sintering stoichiometric amounts of FeV_2O_4 and MnV_2O_4 in evacuated quartz tubes at 1050 °C for 60 hours. FeV_2O_4 and MnV_2O_4 were prepared under similar conditions from stoichiometric amounts of FeO, MnO, V_2O_5, and V powders. Chemical homogeneity and composition of these samples were checked by energy dispersive x-ray (EDX) spectroscopy. The cubic cell lattice parameter of $Fe_{1-x}Mn_xV_2O_4$ was found to increase linearly with increasing x, i.e., obeying Vegard's law. Temperature-dependent synchrotron x-ray diffraction measurements were performed at BL-8, Photon Factory, KEK, and at BL44B2 [24], SPring-8, Japan. Lattice parameters and atomic positions for selected compounds were obtained from Rietveld refinements. Magnetocaloric effects were evaluated from isothermal *M*-*H* data by using Maxwell's relation.

For each of the isothermal *M*-*H* measurements in a field-increasing run, the sample was first heated well above the ferrimagnetic transition temperature T_{N1} to ensure a complete conversion to a paramagnetic state, and then cooled down to the desired measurement temperature. This protocol has proven to be indispensable to accurately evaluate magnetocaloric quantities for first-order as well as second-order magnetic transitions [25].

In Fig. 3(a), we show the temperature dependence of magnetizations of $Fe_{1-x}Mn_xV_2O_4$ compounds with $H = 0.3$ T. The data clearly show two magnetic transitions: one corresponding to T_{N1} and the other corresponding to T_{N2}. According to the previous neutron-diffraction experiments for FeV_2O_4 and MnV_2O_4 [12,26], T_{N1} is assigned to the ferrimagnetic transition of Fe or Mn and V spins, while T_{N2} is found to be the canting transition of V spins although the ordered pattern of the transverse moment appears to be different between them. In view of the systematic variation in T_{N2} and the magnetization at low temperatures, it is reasonable to interpret T_{N2} to be the canting transition of V spins also for the solid-solutions similar to the end compounds. As x increases, T_{N1} decreases monotonically while T_{N2} shows nonmonotonic variation, taking a minimum at $x = 0.6$. The magnetization of the $x = 1.0$ compound turns out to decrease at a temperature slightly below T_{N2}. This behavior has commonly been observed in previous studies [26–29], and the origin has been assigned to the influence of the V orbital angular momentum [26].

To reveal the structural phase diagram, we also performed extensive measurements of temperature-dependent synchrotron x-ray diffraction. In Fig. 4(a), we show the temperature variation of the c/a ratio for selected samples with $0.4 \leqslant x \leqslant 0.8$. For $x \leqslant 0.6$, the c/a ratio clearly begins to deviate from unity and increase at T_{N1} as determined from magnetization measurements, and then turns to decrease at T_{N2}. For $x = 0.8$, c/a remains at unity below T_{N1}, but starts to decrease at T_{N2}. Based on these temperature-dependent
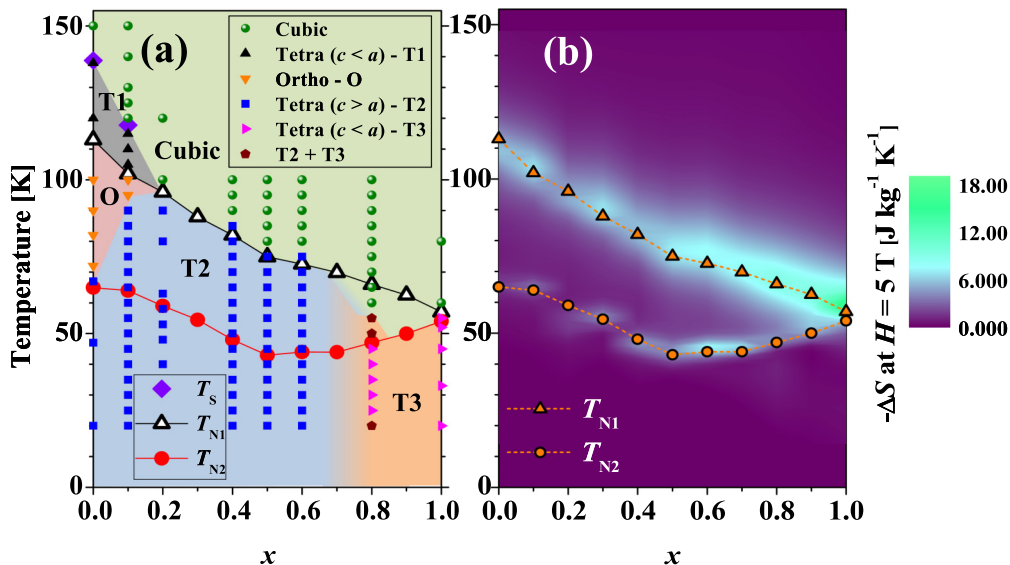
FIG. 2. (Color online) (a) Magnetic and structural phase diagram of $Fe_{1-x}Mn_xV_2O_4$. (b) Contour plot of the magnetocaloric effect or isothermal entropy change ($-\Delta S$) of $Fe_{1-x}Mn_xV_2O_4$ for a field change from 0 to 5 T.
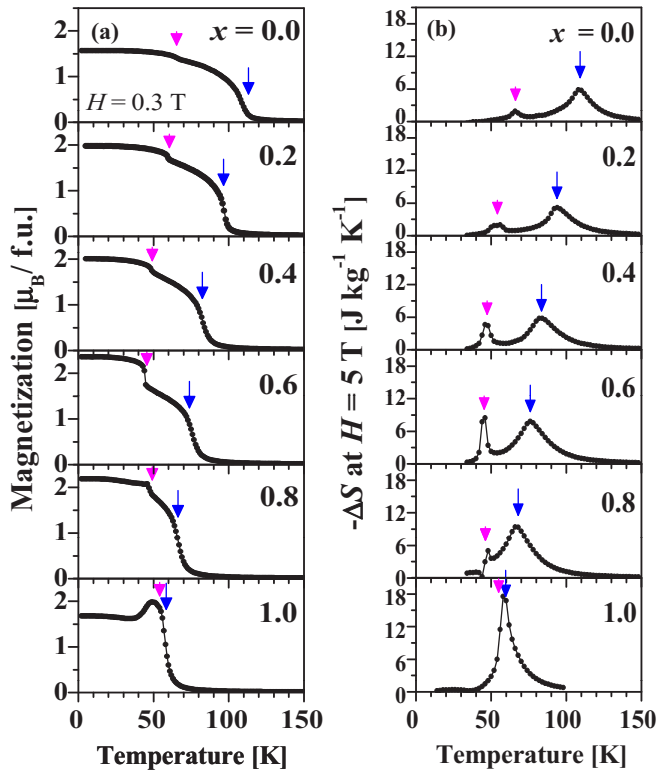
FIG. 3. (Color online) Temperature dependence of (a) magnetization at $H = 0.3$ T and (b) magnetocaloric effect ($-\Delta S$) for a field change from 0 to 5 T for selected samples of $Fe_{1-x}Mn_xV_2O_4$. The blue and purple arrows indicate the ferrimagnetic (T_{N1}) and V spin-canting (T_{N2}) transitions, respectively.

FIG. 4. (Color online) (a) Temperature dependence of the ratio of the c-axis and the a-axis lattice parameters for several samples. (b) The ratio of V–O bond length along the c axis and within the ab plane ($\equiv Q$) is plotted against temperature for several x members of $Fe_{1-x}Mn_xV_2O_4$. ΔQ denotes the difference between the Q values at low temperature and that just above T_{N2}, as indicated by dashed lines. The respective Q values above the ferrimagnetic (T_{N1}) transition ($=1$) are also indicated by a dashed line as a reference. Both in panels (a) and (b), blue and purple arrows indicate the ferrimagnetic (T_{N1}) and V spin-canting (T_{N2}) transitions, respectively.

structural and the magnetization data, we constructed a phase diagram of $Fe_{1-x}Mn_xV_2O_4$, as shown in Fig. 2(a).

As clearly seen in this phase diagram, T_{N1} decreases gradually and monotonically from 113 to 57 K as x increases from 0 to 1.0. T_{N2} also decreases with increasing x, but it turns to increase at around $x = 0.6$ and almost merges with T_{N1} at $x = 1.0$. The structural aspect appears to be more complex. For $x = 0$ and 0.1 compounds, successive structural transitions are observed: The first transition from cubic C to the T1 phase occurs in the paramagnetic phase, due to Jahn–Teller-type compression of FeO_4 tetrahedra along the c axis, where compression is favored over elongation by lattice anharmonicity [7,10,11]. This transition temperature rapidly decreases as x is increased, and the T1 phase disappears for $x \geqslant 0.2$. The structural transition from T1 to orthorhombic O phase below T_{N1} in $x = 0.0$ and 0.1 arises from the spin-orbit interaction of Fe^{2+} in the magnetically ordered phase [11]. Below T_{N1}, Fe spins lie within the ab plane of the T1 phase, and the spin-orbit interaction stabilizes an elongated FeO_4 tetrahedra perpendicular to the compressed c axis of the T1 phase, leading to an intermediate O phase. Further lowering of the temperature causes a subsequent transition to a low-temperature tetragonal (T2) phase with $c > a$, where the elongated axis (i.e., c axis) lies in the ab plane of the T1 phase, parallel to the net magnetization. As orbitally active Fe^{2+} is progressively substituted with orbitally inactive Mn^{2+}, the lattice anharmonicity becomes weaker while the spin-orbit

interaction remains almost unaffected. This x dependence governs the Jahn–Teller distortion pattern [7], resulting in complete disappearance of T1 and O phases and instead stabilization of the T2 phase below T_{N1} for $x \geqslant 0.2$ [30]. For x less than around 0.7, the global crystal structure below T_{N1} is dominated by the Jahn–Teller and spin-orbit interactions of the A site, and below T_{N2}, the effect of the V site becomes significant [31]. Similar to FeV_2O_4 [11], t_{2g} electrons at V sites appear to undergo ferroic-orbital ordering [32], accompanied by the reduction of the c-axis lattice parameter due to the compression of VO_6.

Upon reaching $x = 0.8$, the averaged Jahn–Teller instability and spin-orbit interaction of the A site is significantly reduced since most of the orbital-active Fe^{2+} is replaced by orbital-inactive Mn^{2+} ions, and the crystal structure is alternatively dominated by Jahn-Teller and exchange interactions of the V site, resulting in a compressed tetragonal (T3) phase with $c < a$ below T_{N2} [33], similar to MnV_2O_4 [11]. For this compound, T_{N2} is not only the spin-canting transition but also coincides with a structural transition. At the composition around $x = 0.7$, the ground state changes from a $c > a$ tetragonal (T2) phase to the $c < a$ tetragonal (T3) phase. In view of the similar temperature dependence of c/a ratio of $x = 0.8$ and 1.0 compounds, we assume that the space group of the T3 phase is $I4_1/a$ as reported previously for MnV_2O_4 [11], which includes two V sites to form an

antiferro-orbital state, and the elongation axes of the two VO_6 octahedra are perpendicular to each other and also to the *c* axis of the compressed unit cell. When the phase diagram is viewed from the MnV_2O_4 side, the concomitant transition temperature T_{N2} decreases upon the partial Fe substitution and the disorder effect may play a role in terms of both the ionic radius and the orbital-dependent exchange and Jahn–Teller interactions.

Given the phase diagram, we next investigate the magnetocaloric effect of $Fe_{1-x}Mn_xV_2O_4$ compounds. In Fig. 3(b), we plot $-\Delta S$ deduced from isothermal *M-H* measurements via Maxwell's relation. For all *x* members except for $x = 1.0$, $-\Delta S$ shows two peaks: one corresponding to T_{N1} and one corresponding to T_{N2}. For $x = 1.0$, the two peaks nearly merge to give rise to a large magnetocaloric value of 18 J kg^{-1} K^{-1}, almost in accord with a previous report [20]. The peak associated with T_{N1} exhibits a rather broad tail, indicating a second-order transition, while the peak associated with T_{N2} shows a rather narrow width, especially for $0.4 \leqslant x \leqslant 0.8$, showing the first-order nature of the spin-canting transition. The $-\Delta S$ peak value at T_{N2} shows nonmonotonic *x* variation: It increases with *x*, reaches a maximum value of 8.5 J kg^{-1} K^{-1} at $x = 0.6$, and then decreases for $x = 0.8$. Thus, the $-\Delta S$ peak values at T_{N1} and T_{N2} are almost comparable for the $x = 0.6$ compound whereas the $-\Delta S$ peak value at T_{N1} is larger than that at T_{N2} for other compounds. The magnetocaloric values are displayed in Fig. 2(b) as a contour plot.

To gain more insight into the observed magnetocaloric effects, we plot in Fig. 5(a) the $-\Delta S$ peak values at T_{N1} and T_{N2} and the sum of them as a function of *x*. The $-\Delta S$ value at T_{N1} increases almost monotonically as *x* is increased, while the $-\Delta S$ value at T_{N2} clearly has a maximum at $x = 0.6$. The behavior of $-\Delta S$ at T_{N1} can be understood in terms of a conventional second-order transition. As shown in

Fig. 5(b), $-\Delta S$ values for $H = 5$ T at T_{N1} appear to depend almost linearly on the square of magnetization at T_{N1} and $H = 5$ T, except for the $x = 1.0$ compound, in agreement with the theoretical prediction of the second-order transitions [34]. A finite intercept should be attributable to the ferrimagnetic nature of the present system. However, such a comparison with the magnetization alone is inadequate for the $-\Delta S$ peak values at T_{N2} since the first-order spin-canting transition is accompanied by orbital ordering of the V electron, and hence local distortion of VO_6 octahedra.

In order to observe the effect of orbital ordering on $-\Delta S$ at T_{N2}, we have determined the local distortion of the VO_6 octahedron via Rietveld analysis of the synchrotron x-ray diffraction data with sufficient data acquisition time at several selected temperatures [35]. In Fig. 4(b), we plot a ratio $Q \equiv (V\text{-}O)_c/(V\text{-}O)_{ab}$ against temperature for several samples. Here, $(V\text{-}O)_c$ and $(V\text{-}O)_{ab}$ stand for the V-O bond length along the *c* axis and within the *ab* plane, respectively. While the orbital ordering is assumed to be different (ferroic for $x \leqslant 0.6$ and antiferroic for $x \geqslant 0.8$), the *Q* value commonly decreases for both phases below T_{N2} due to the compression of the octahedron along the *c* axis for $x \leqslant 0.6$ and the elongation within the *ab* plane for $x \geqslant 0.8$. As a measure of the VO_6 distortion, we defined ΔQ to be the difference between the *Q* values at the lowest temperature and that just above T_{N2}, as shown in Fig. 4(b). Clearly, ΔQ is largest for the $x = 0.6$ compound.

In Fig. 5(c), we plot $-\Delta S$ peak values at T_{N2} against $|\Delta Q|^2$. It shows a linear dependence with a finite intercept, implying two contributions. The entropy change that depends linearly on the square of the VO_6 distortions should be attributed to the lattice contribution. The other one corresponding to the intercept is a magnetic contribution related to the increase
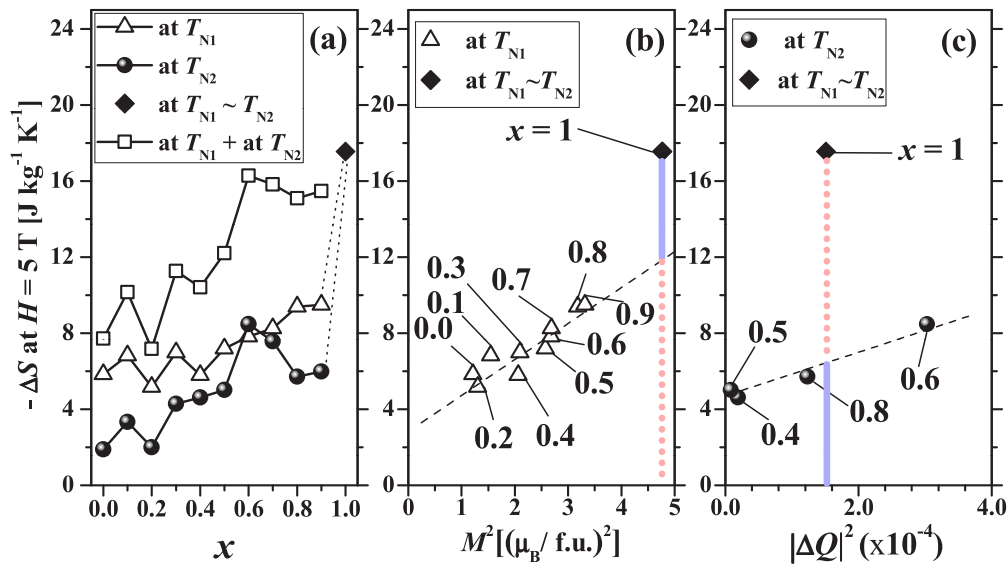
FIG. 5. (Color online) (a) Mn concentration (*x*) dependence of the peak value of the magnetocaloric effect associated with the ferrimagnetic (T_{N1}) and V-spin canting (T_{N2}) transitions in $Fe_{1-x}Mn_xV_2O_4$. The sum of them is also plotted. (b) Magnetocaloric peak values at T_{N1} are plotted against the square of the magnetization at T_{N1} and at $H = 5$ T. (c) Magnetocaloric peak values at T_{N2} are plotted against square of magnitude of the distortion (ΔQ) of the VO_6 octahedra across the V-spin-canting transitions. For the definition of ΔQ, see main text. In panels (b) and (c), the ferrimagnetic (light-red dotted lines) and spin-canting-plus-lattice (light-blue solid lines) contributions to $-\Delta S$ of MnV_2O_4 at $T_{N1} \sim T_{N2}$ are also indicated.

in the net magnetization at T_{N2} due to the V spin cantings. Therefore, nonmonotonic x variation of $-\Delta S$ at T_{N2} arises from the enhanced local distortion of VO_6 octahedra around $x = 0.6$. Furthermore, Figs. 5(b) and 5(c) indicate that the large magnetocaloric value of $x = 1.0$ at $T_{N1} \sim T_{N2}$ considerably deviates from the respective dependency, but can be expressed approximately as the sum of the entropy release of the two transitions; $-\Delta S$ (observed) = 12 (ferrimagnetic, at T_{N1}) + 6 (spin canting + lattice, at T_{N2}) = 18 J kg^{-1} K^{-1}.

In summary, the magnetic and structural phase diagram has been revealed for $Fe_{1-x}Mn_xV_2O_4$ compounds with spinel structure. Subtle interplay of Jahn–Teller, spin-orbit, and exchange interactions of Fe, Mn, and V sites has given rise to a rich phase diagram. Moderately large magnetocaloric values have been observed, associated with both the ferrimagnetic transition and the concomitant spin-canting and orbital-ordering transition. The enhanced value found for MnV_2O_4 has been attributed to the sum of these two entropy changes.

[1] D. B. Rogers, R. J. Arnott, A. Wold, and J. B. Goodenough, J. Phys. Chem. Solids **24**, 347 (1963).

[2] P. G. Radaelli, New J. Phys. **7**, 53 (2005).

[3] S. Di Matteo, G. Jackeli, and N. B. Perkins, Phys. Rev. B **72**, 020408(R) (2005).

[4] S. H. Lee *et al.*, J. Phys. Soc. Jpn. **79**, 011004 (2010).

[5] Y. Kato, G. W. Chern, K. A. Al-Hassanieh, N. B. Perkins, and C. D. Batista, Phys. Rev. Lett. **108**, 247215 (2012).

[6] J. Matsuno, T. Mizokawa, A. Fujimori, D. A. Zatsepin, V. R. Galakhov, E. Z. Kurmaev, Y. Kato, and S. Nagata, Phys. Rev. B **55**, R15979 (1997).

[7] S. Ohtani, Y. Watanabe, M. Saito, N. Abe, K. Taniguchi, H. Sagayama, T. Arima, M. Watanabe, and Y. Noda, J. Phys.: Condens. Matter **22**, 176003 (2010).

[8] J. Kanamori, J. Appl. Phys. **31**, S14 (1960).

[9] Even in the cubic structure, there is a trigonal distortion of VO_6 octahedra, but the energy-level splitting is not significant when compared with the energy scale of temperature.

[10] T. Katsufuji, T. Suzuki, H. Takei, M. Shingu, K. Kato, K. Osaka, M. Takato, H. Sagayama, and T. Arima, J. Phys. Soc. Jpn. **77**, 053708 (2008).

[11] Y. Nii, H. Sagayama, T. Arima, S. Aoyagi, R. Sakai, S. Maki, E. Nishibori, H. Sawa, K. Sugimoto, H. Ohsumi, and M. Takata, Phys. Rev. B **86**, 125142 (2012).

[12] G. J. MacDougall, V. O. Garlea, A. A. Aczel, H. D. Zhou, and S. E. Nagler, Phys. Rev. B **86**, 060414(R) (2012).

[13] S. Sarkar and T. Saha-Dasgupta, Phys. Rev. B **84**, 235112 (2011).

[14] S. Sarkar, T. Maitra, R. Valenti, and T. Saha-Dasgupta, Phys. Rev. Lett. **102**, 216405 (2009).

[15] T. Suzuki, M. Katsumura, K. Taniguchi, T. Arima, and T. Katsufuji, Phys. Rev. Lett. **98**, 127203 (2007).

[16] J. H. Chung, J. H. Kim, S. H. Lee, T. J. Sato, T. Suzuki, M. Katsumura, and T. Katsufuji, Phys. Rev. B **77**, 054412 (2008).

[17] H. Tsunetsugu and Y. Motome, Phys. Rev. B **68**, 060405(R) (2003).

[18] O. Tchernyshyov, Phys. Rev. Lett. **93**, 157206 (2004).

[19] D. I. Khomskii and T. Mizokawa, Phys. Rev. Lett. **94**, 156402 (2005).

[20] X. Luo, Y. P. Sun, L. Hu, B. S. Wang, W. J. Lu, X. B. Zhu, Z. R. Yang, and W. H. Song, J. Phys.: Condens. Matter **21**, 436010 (2009).

[21] K. A. Gschneidner, Jr., V. K. Pecharsky, and A. O. Tsokol, Rep. Prog. Phys. **68**, 1479 (2005).

[22] E. Liu *et al.*, Nat. Commun. **3**, 873 (2012).

[23] J. Liu, T. Gottschall, K. P. Skokov, J. D. Moore, and O. Gutfleisch, Nat. Mater. **11**, 620 (2012).

[24] K. Kato, R. Hirose, M. Takemoto, S. Ha, J. Kim, M. Higuchi, R. Matsuda, S. Kitagawa, and M. Takata, AIP. Conf. Proc. **1234**, 875 (2010).

[25] L. Caron, Z. Q. Ou, T. T. Nguyen, D. T. Cam Thanh, O. Tegus, and E. Bruck, J. Magn. Magn. Mater. **321**, 3559 (2009).

[26] V. O. Garlea, R. Jin, D. Mandrus, B. Roessli, Q. Huang, M. Miller, A. J. Schultz, and S. E. Nagler, Phys. Rev. Lett. **100**, 066404 (2008).

[27] V. Hardy, Y. Breard, and C. Martin, Phys. Rev. B **78**, 024406 (2008).

[28] H. D. Zhou, J. Lu, and C. R. Wiebe, Phys. Rev. B **76**, 174403 (2007).

[29] K. Adachi, T. Suzuki, K. Kato, K. Osaka, M. Takata, and T. Katsufuji, Phys. Rev. Lett. **95**, 197202 (2005).

[30] Rietveld refinement results indicate the crystallographic symmetries of the cubic, T1, O, and T2 phases to be $Fd-3m$, $I4_1/amd$, $Fddd$ and $I4_1/amd$, respectively. See Supplemental Material at http://link.aps.org/supplemental/10.1103/PhysRevB.89.104427 for the representative result. Also, results for the $x = 0.1$ compound indicate negligibly small intersite mixing between the Fe and V sites.

[31] Two-step reduction of VO bond length along c direction was observed, indicating that the distortion of VO_6 octahedra below T_{N1} is mainly driven by the distortion of neighboring AO_4 tetrahedra via the elastic interaction while additional compression of VO_6 below T_{N2} is due to the V-orbital ordering.

[32] Using convergent-beam electron diffraction for $x = 0.6$ compound, we have confirmed that mirror and d-glide symmetries are preserved below T_{N2}, indicating the ferro-orbital nature of the transition, similar to FeV_2O_4.

[33] For the $x = 0.8$ compound, we observed phase separation into the T2 and T3 phases slightly above T_{N2} and also at 20 K. Tiny changes of crystal field splitting associated with the thermal

contraction might possibly affect the competition of almost-degenerate T2 and T3 phases, leading to the phase separation.

[34] E. Z. Valiev, Phys. Met. Metallogr. (Transl. of Fiz. Met. Metalloved.) **104**, 8 (2007).

[35] The c/a ratio represents the global lattice distortion, whereas what should be compared with the magnetocaloric effect is the local distortion of VO_6 octahedra which does not necessarily coincide with the global lattice distortion [11].